II Functional and anatomical features of *Apis mellifera* olfactory interneurons

Abstract

Natural olfactory stimuli occur as mixtures of many individual compound odors. Since the honeybee exhibits an elaborate behavior comprising sophisticated olfactory learning tasks, we studied the representation of odor mixtures in relation to neural morphology within its brain. To understand mixture representation within the honeybee brain we performed electrophysiological recordings of single olfactory interneurons within the first-order relay station of the olfactory pathway, the antennal lobe. Antennal lobe-intrinsic and output neurons showed different odor identity and odor mixture encoding strategies, presumably caused by their morphological arborizations. Antennal lobe output neurons of the lateral antenno-cerebral tract (lACTs) convey odor mixture information onto the second-order relay station of the olfactory pathway, the mushroom bodies whereas antennal lobe output neurons of the median antenno-cerebral tract (mACTs) transfer odor identity information. The 3-D composition of single l-, and mACTs within a spatial reference map, the 'Atlas of the Honeybee Brain', revealed their uniglomerular input functionally represented by glomerulus-specific olfactory response profiles. The spatial distribution of their axon terminals (boutons) within their output region, the mushroom body lips appeared largely segregated between l- and mACTs. The mACTs among themselves innervated the same anatomical region of the mushroom body lips but with a different bouton density. Thus our results show that glomerulus-specific

input within the antennal lobe is either represented by an area-dependent (lACTs) or a density-dependent (mACTs) bouton topography within the mushroom body lips.

Introduction

Most naturally occurring odors are complex blends consisting of a large number of volatile compounds (Pichersky and Gershenzon, 2002) and virtually all animal species have evolved sophisticated mechanisms to extract meaningful information from their complex living space. In recent years it has been shown that perception of an odor mixture is either dominated by its most effective component or the mixture acquires a new identity (Staubli et al., 1987; Derby et al., 1996; (Wiltrout et al., 2003); Tabor et al., 2004; Deisig et al., 2006). Thus, single-odor responses might interact in the response to the mixture, leading to a neural representation that discards information about individual components but acquires mixture-specific properties.

Functional studies capturing the response of single olfactory neurons and individual glomeruli to simple chemical compounds showed that odor identity is encoded by spatio-temporal activity patterns within the first-order relay station of the olfactory pathway; the olfactory bulb (OB) in vertebrates (Cinelli and Kauer, 1995; Friedrich and Korsching, 1997; Friedrich and Korsching, 1998; Rubin and Katz, 1999; Lam et al., 2000; Uchida et al., 2000; Meister and Bonhoeffer, 2001) and its insect analog, the antennal lobe (AL) (Joerges et al., 1997; Galizia et al., 1999; Sachse et al., 1999; Galizia and Menzel, 2000). Even simple chemical compounds as, for example, odor molecules containing short hydrocarbon chains and a few functional groups generate widespread activity patterns within the OB / AL that encompass large sets of receptor types and corresponding glomeruli (Rubin and Katz, 1999; Uchida et al., 2000; Meister and Bonhoeffer, 2001). An extrapolation to complex chemical cues would there-

fore predict the recruitment of overlapping fractions of receptor types and their corresponding glomeruli. Thus the amazing specificity of olfactory recognition requires the ability for the brain to discriminate large and complex combinations of glomerular activities, a process that could be facilitated by the extensive interactions between glomeruli.

Based on the study of OB glomerular responses to natural scents, Lin et al. (2006) showed that glomerular responses to natural odors are remarkably sparse. Studies on insects, particularly on the honeybee, support this result by showing that mixture responses do not represent a simple linear sum of the responses elicited by the mixture components (Joerges et al., 1997; Deisig et al., 2006). Considering the OB / AL output neurons the mitral cells (MCs) in vertebrates and the projection neurons (PNs) in insects, it has been shown that mixture responses were either dominated by one of the component responses (Tabor et al., 2004) a phenomenon referred to as hypoadditive mixture interactions (Duchamp-Viret et al., 2003) or revealed suppressive mixture interactions (Sachse, 2002). Hence these effects were not observed in afferent glomeruli activity patterns they are considered to arise within the OB / AL affected by circuit interactions (Friedrich and Laurent, 2004). Thus this present study was designed to characterize single olfactory interneuron (projection neurons and local interneurons) response profiles and to address the issue of how odor identity and mixtures are encoded within the AL neuronal space.

Odors are encoded within the insect olfactory system by the activity of ensembles of neurons. In the honeybee *Apis mellifera*, 60,000 olfactory sensory neurons (OSNs) are located in antenna sensilla (Esslen and Kaissling, 1976) and process olfactory information to the AL through four tracts (T1-T4) (Suzuki, 1975). OSN axons converge onto 4000 AL intrinsic local interneurons (LNs) (Witthoeft, 1967; Fonta et al., 1993) and 800 projection neurons (PNs) (Bicker et al., 1993) which represent the AL output. Synaptic information processing between OSNs, LNs and PNs takes place within areas of high synaptic densi-

ties, the AL glomeruli (Gascuel and Masson, 1991). The honeybee AL consists of about 160 glomeruli, each representing a morphological and functional sub-unit identified by the antennal tract which innervates it (T1-T4) (Arnold et al., 1985; Galizia et al., 1999). From the AL olfactory information is transferred to the lateral protocerebrum (LH) and the mushroom bodies (MBs) via three distinguishable antenno-cerebral tracts (ACTs) (Mobbs, 1982). Multiglomeru-lar cells leave the AL via the medio-lateral ACT (mlACT), terminating solely in the LH, whereas uniglomerular PNs leave the AL through the lateral and median ACT (l- and mACT) projecting onto the LH and the MBs (Abel et al., 2001), which are higher-order sensory integration centers which play a dominat role in odor learning (Heisenberg, 1998; Menzel, 1999). The MBs receive input from different sensory modalities projecting onto spatially distinct areas of the MB calyces (Mobbs, 1982; Gronenberg, 2001; Schroeter and Menzel, 2003). Olfaction is known to be confined to the MB lip region (Mobbs, 1982).Within the MB lip, olfactory information is synaptically transferred from the PNs onto 170,000 Kenyon cells (KC) which themselves converge onto MB output neu-rons (Mobbs, 1982; Rybak and Menzel, 1993).

Thus within the honeybee brain olfactory information is conveyed from the AL onto the MBs via two parallel pathways (l- and mACT), indicating different odor-encoding strategies associated with their distinct morphology. Mueller et al. (2002) suggested that l- and mACT represent two odor processing channels by encoding different features of the same odor. This dual coding strategy might ,in turn, be related to their dissimilar anatomical features regarding their input (AL) as well as their output site (MBs). lACT PNs receive their input from the T1 glomeruli, whereas mACT PNs from the T2, T3 and T4 glomeruli. Tracing of multiple PNs revealed that l- and mACT output represented by their axon terminal (boutons) arborization patterns remain largely segregated within the MBs and the LH (Gronenberg, 2001; Kirschner et al., 2006).

Since it is known that individual PNs differ with respect to their odor-encoding

properties and their spatial anatomical organization, this study was designed to correlate functional and anatomical features on the level of single lACT and mACT PNs. Besides their encoding of odor identity and odor mixtures, we addressed the issue of their anatomical organization within a spatial reference map, the Atlas of the Honeybee Brain (Brandt et al., 2005; see also `http://www.neurobiologie.fu-berlin.de/beebrain`). A combination of electrophysiological recording, intracellular staining, immunohistochemistry and 3-D reconstruction elucidate functional and anatomical features of single l- and mACT PNs within the entire network. We could show that l- and mACT represent two olfactory processing channels with mixture-specific coding properties correlated to their anatomical input within the AL and their output within the MBs.

Materials and Methods

Honeybees

Worker bees (*Apis mellifera carnica*) were caught at the hive entrance or in an indoor flight room, immobilized by cooling, and mounted in plastic tubes. The bees were fed with sucrose solution and kept in the dark at $20\,°C$ and high humidity. On the following day, the head was fixed with wax and opened between the median ocellus and the base of the antennae. Glands and tracheal sheaths were removed. A second hole was cut to expose the esophagus. The brain was kept wet at all times by dribbling drops of bee physiological saline solution onto (in mmol^{-1}: 130 NaCl, 6 KCl, 2 $MgCl_2$, 10 HEPES, 17 glucose, 6 fructose, 160 sucrose, pH 6.7).
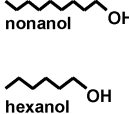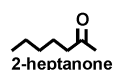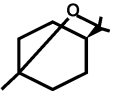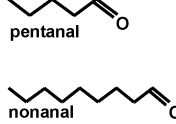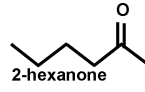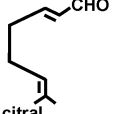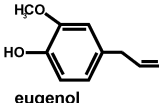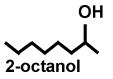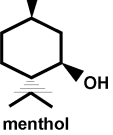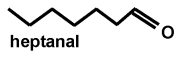
alcohol	ketone	terpene	aldehyde	benzene	mixture
nonanol — OH hexanol — OH	2-heptanone				**A**
		1,8 cineole	pentanal nonanal		**B**
	2-hexanone	citral (CHO)		eugenol	**C**
2-octanol (OH)		menthol (OH)	heptanal		**D**

Figure II.1:
Tertiary mixtures and their elemental components assigned to their functional group.

Electrophysiology

Glass electrodes were pulled with a horizontal laser puller (P-2000 Sutter Instruments, Novarto, CA) and their tips were filled with 4 % tetramethylrhodamin-biotin dextran (Micro-Ruby; Invitrogen, Germany) in 0.2 M potassium acetate. The electrodes (resistance as measured in the tissue ranged from 120 to 200 MΩ) were positioned at the top of the AL, and lowered posteriorly into the neuropil until a neuron could be penetrated by using a micromanipulator (Leitz). A reference electrode, a chlorized silver wire, was inserted into the eye. The recordings were done in bridge mode using an intracellular BRAMP 1 amplifier (NPI Electronics, Tamm, Germany). Data were long-pass filtered at 26 Hz, digitized using a 1401 interface and stored on a PC using spike2 version 2.5 software (Cambridge Electronic Design, UK).

Stimulation

The animal's antennae were exposed to a constant active charcoal-filtered stream of room air (airflow rate 10 ml/s) guided through a glass tube with an inner diameter of 14 cm placed 1 cm from the antenna. The control stimulus was a glass syringe plus filter paper with mineral oil (Sigma-Aldrich, Germany) delivering a constant airflow rate of 10 ml/s. For each odor, 4 μl were placed on a filter paper in a glass syringe which was introduced into the continuous air stream. To avoid mechanical stimulation a computer-controlled valve switched between control stimulus and odor-loaden syringe such that the antenna was always exposed to an air stream with a flow rate of 20 ml/s.

The stimulus timing was computer-controlled and each odor stimulation lasted for 2 s. All odors were diluted 1:10 in mineral oil and checked for purity and mixture composition by gaschromatography (GC; Trace GC Ultra, Thermo, Electron Corporation, Waltham, MA, USA). The animals received single compound odors, tertiary odor mixtures of the single compound as well as complex mixtures (Sigma-Aldrich, Germany). Figure 1 shows the four tertiary mixtures and their elemental components representing different complexities. Mixture A was composed of the blossom components nonanol and hexanol as well as 2-heptanone, which is known to function as an alarm pheromone in bees (Balderrama et al., 2002). Mixture B contained the single components pentanal, nonanal (both are parts of the communication system of other species as beetles and ants; Phillips et al., 1993; Keegans et al., 1993), and 1,8 cineole, representing a natural plant blend. Mixture C consisted of citral, a honeybee pheromone pardo1994, the blossom component 2-hexanone which is similar to the pheromonal component 2-heptanone, and clove oil, represented by its major component eugenol. Mixture D was composed of 2-octanol (similar the the honeybee pheromone 1-octanol, Balderrama et al., 1996), heptanal, which is known to be involved in wasp communication (Fortunato et al., 2001), and the

natural floral blend peppermint, represented by its major component menthol.

In some animals multiple-trial presentations of the same odor were used to account for response variability, whereas in other animals one-trial presentation of different odors (between 4 and 30) performed in a randomized fashion (to exclude sequence effects) revealed the number of odors which elicited a response (odor generalization). Therefore the number of odors tested varies across animals.

Recordings lasted between 10 and 20 minutes and therefore a fixed interstimulus-interval could not be maintained.

The large and diverse odor repertoire allowed me to address the issue of encoding odor identity (functional groups), odor quality (pheromones, natural blends) and odor mixtures.

Intracellular staining and histology

Micro-Ruby was iontophoretically injected by using depolarizing current pulses of and $0.2\,\mathrm{s}$ duration applied at $1 - 2\,\mathrm{Hz}$. Complete labeling of neurons required continuous dye injection for at least $15\,\mathrm{minutes}$ with a current between $2\,\mathrm{nA}$ and $3\,\mathrm{nA}$. After intracellular filling, Micro-Ruby was allowed to diffuse from 3 hours up to overnight. After dissection, the brains were fixed in $4\,\%$ formaldehyde diluted in $50\,\%$ methanol for 24 hours at $4\,^{\circ}\mathrm{C}$. Preparations were rinsed for $10\,\mathrm{minutes}$ in $0.1\,\mathrm{M}$ phosphate-buffered saline (PBS; pH 6.7), dehydrated in an increasing ethanol series ($30\,\%$, $50\,\%$, $70\,\%$, $90\,\%$, $99\,\%$, $100\,\%$, $10\,\mathrm{minutes}$ each), degreased in xylol for 5 minutes, and rehydrated in a decreasing ethanol series. Brains were then washed for $10\,\mathrm{minutes}$ in PBS and blocked in $10\,\%$ normal goat serum (NGS; Sigma-Aldrich, Germany) in PBS for $30\,\mathrm{minutes}$ at room temperature. Subsequently, preparations were incubated in a primary antiserum composed of SYNORF1 and NC42 (Klagges et al., 1996), diluted 1:10 in PBS for 48 hours at $4\,^{\circ}\mathrm{C}$. The primary antibodies originate from a screen

of Drosophila synapse proteins and were kindly provided by Dr. E. Buchner (Wuerzburg, Germany). To intensify the intracellular staining of the recorded neuron, streptavidin-Cy3 (Invitrogen, Germany) diluted 1:250, was added to the primary antiserum. Brains were rinsed in PBS for 15, 30, 45, and 60 minutes and then incubated for 24 hours with a Cy5-conjugated mouse anti-rabbit secondary antibody (Jackson Immunoresearch, West Grove, PA; dilution 1:500 in PBS). After another four rinses in PBS for 15, 30, 45, and 60 minutes, brains were dehydrated in an increasing ethanol series, precleared in a mixture of 30 % methyl-salicylate (MS) and 100 % ethanol, and mounted as whole mounts in MS in double-sided custom slides.

Data analysis

Electrophysiological data processing

MATLAB and the MATLAB Statistics Toolbox (The MathWorks, Inc.) were used for the analysis of the electrophysiologically-recorded data. All analyses were accomplished for m- and l-ACT projection neurons (mACT N = 23, lACT N = 7) as well as for local interneurons (LNs N = 7). Neurons were identified either by their anatomy after intracellular filling, or by their spike patterns and depth of the recording. For detecting an odor-evoked response we first constructed the ISI distribution of spontaneous activity. We therefore collected all interspike-intervals (ISI) during a 1 s long interval before stimulus onset. These were pooled across all trials independent of the stimulus. In each single trial we then collected the ISIs during 1 s after stimulus onset and tested this sample against the ISI spontaneous distribution using a Wilcoxon rank-sum test (p = 0.05). Significant changes were defined as either excitatory (1), or inhibitory (-1). Non-significant changes were defined as a neutral response (0).

If no ISI could be detected in either the spontaneous or the response window it was defined as a neutral reponse (0). For non-stationary recordings due to

long-term change in the spontaneous activity level response detection and classification had to be performed manually. To quantify the response reliability across multiple trials of the same odor stimulus we defined the reliability index r as the fraction of trials that exhibited a response. We defined the generalization index g of a neuron as the relative number of odors that evoked either an excitatory or inhibitory response where response ISI had been pooled across all trials of identical stimuli. The response strength for a particular odor was determined by the average firing rate during odor stimulation (2 s duration) subtracted by the average rate prior to stimulation (1 s). Time-resolved estimates of the dynamic response profile were obtained by means of kernel convolution (Parzen, 1962; Nawrot et al., 1999. For a given spike train $t_1, \cdots, t_n$ the convolution integral

$$\hat{r}(t) = \int d\tau\, \omega(\tau) \cdot \delta(t - \tau)$$

returns the rate as function of trial time. The integral over the δ function is unity only at instances $t = t_i$ that represent a spike event. The kernel function ω was chosen either as a triangular function or an alpha function defined on a finite support. The kernel width was parameterized by its standard width σ (Nawrot et al., 1999).

Estimates of the average response latency (lat) of a neuron were obtained as follows. We first pooled spike trains from all trials of all stimuli that yielded a significant positive response. We then estimated the trial-averaged rate function for each of these stimuli before averaging across odors. Finally we performed a threshold detection of the rate function during the stimulus presentation. The threshold was defined as mean ± 5 times standard deviation of the average spontaneous firing rate before stimulus onset. To test for the significant difference in the average response latency of neurons that belong to different neuron classes (mACTs, lACTs, LNs) we applied the Wilcoxon rank sum test.

To ascertain different types of mixture interactions we applied a classification

by Duchamp-Viret et al. (2003), dividing each neuronal response to the mixture into three categories: higher (synergy), equal (hypoadditivity) or lower (suppression) than the strongest response to any of the three elemental components. To quantify the response difference between mixture and most effective component we measured the respective spike counts S_{mix}, S_{max} within a fix window from 200 ms to 1000 ms after stimulus onset and calculated its normalized difference as

$$\kappa = \frac{S_{mix} - S_{max}}{S_{mix} + S_{max}}$$

0 defines no deviation between odor mixture and most effective odor response whereas -1 indicates the highest deviation between these two.

Anatomical data processing

Confocal microscopy and reconstruction   Wholemount preparations were imaged with a a confocal laser scanning microscope (Leica TCS SP2) with a Leica HC PL Apo $20 \times$ /0.7 dry lens objective. Projection neurons were scanned in 2×2 tiled stacks of 350 optical sections with a resolution of 1024×1024 pixels and a voxel size of $0.73 \times 0.73 \times 2 \, \mu$m. Cy3 was excited by using the 543 nm line of a HeNe laser and scanned as the first channel. Cy5 was excited with the 633 nm line of a HeNe laser and scanned as the second channel. For the reconstruction of the innervated neuropil, the scans of the second channel were resampled to lateral dimensions of 512×512 pixel. In the case of tiled images, stacks were combined with the Merge module in Amira (Mercury Computer Systems, Inc, San Diego, CA). Neuropil outlines were then traced with Amira's segmentation editor. Precise automatic geometric reconstruction of neuronal morphology was performed on single confocal image stacks by using a custom module in Amira (Schmitt et al., 2004; Evers et al., 2005). The reconstruction algorithm provided a structural description of the neurons referred to as "skeleton trees", including the topology and the

exact dendritic lengths and diameters. Single projection neuron skeleton trees were fitted into the Atlas of the Honeybee Brain (Brandt et al., 2005, see also `http://www.neurobiologie.fu-berlin.de/beebrain`). Elastic registration was accomplished by applying a $27 \times 27 \times 27$ dimensional control point grid for m- and lACT PNs respectively.

Neuronal architecture within the Atlas of the Honeybee Brain   The overall neuronal architecture and sites of synaptic contacts, here the PN boutons, were analyzed according to their spatial distribution within the Atlas of the Honeybee Brain. By means of the intracellular filling reconstructed generalized cylinders of the PN skeleton trees were identified as sites of synaptic contact in that case swellings along the axonal branches (boutons). Each PN skeleton tree was mapped onto the mushroom lip label field of the honeybee Atlas by using custom modules kindly provided by Jan-Felix Evers (University of Cambridge, UK). Boutons of single PNs within the MB lips of the honeybee Atlas were color-coded and visualized according to their spatial distribution.

Results

Odor encoding in single olfactory interneurons

Response reliability   Since it is known that odor identity is encoded by means of spatio-temporal activity patterns within the AL space (Joerges et al., 1997; Sachse et al., 1999; Galizia et al., 1999; Galizia and Menzel, 2000) the present study was designed to elucidate this combinatorial code on the level of single olfactory interneurons. We used a large and chemically diverse set of odors to characterize the odor response profiles of olfactory interneurons (m-, lACTs, LNs). To account for response variability we accomplished experiments with multiple-trial presentations of one odor and calculated the reliability index r for each neuron (see Material and Methods). Figure 2 shows examples for olfac-
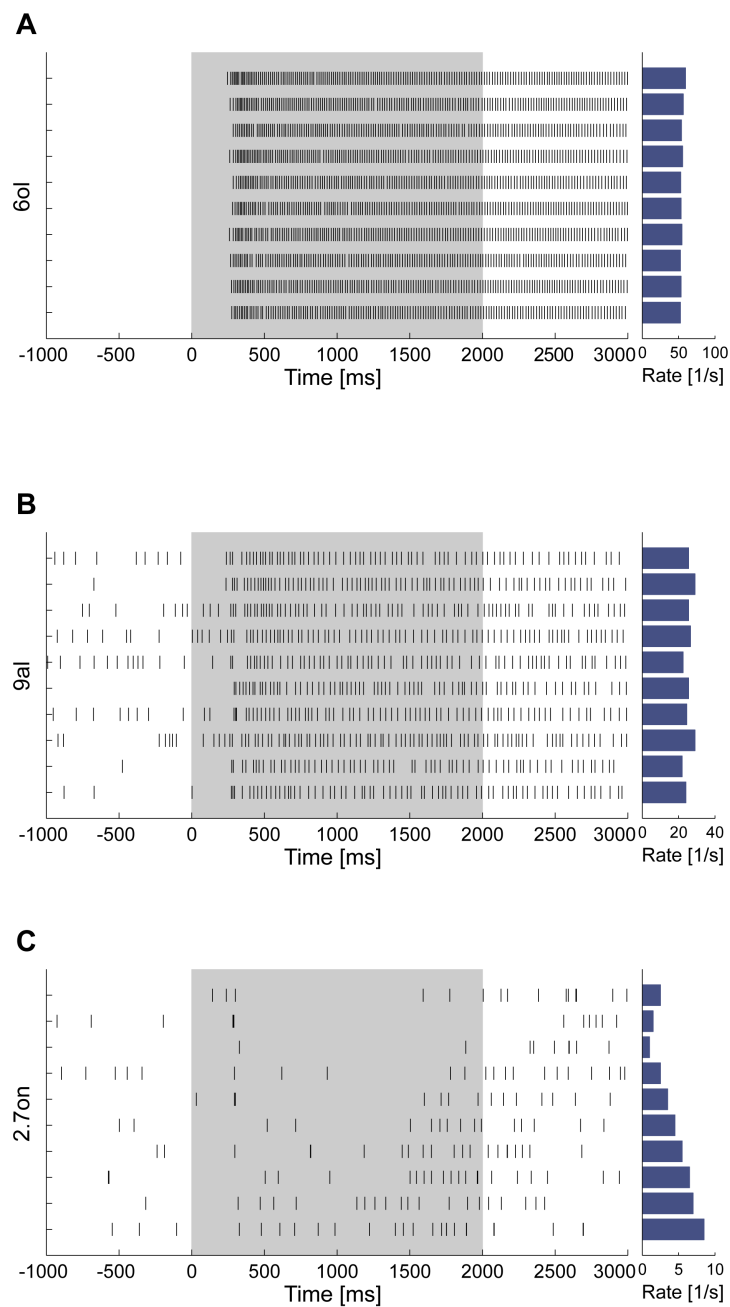
Figure II.2:
Response reliability dot displays. Each tick mark of the dot display represents the occurrence of one spike, each line comprises the spike train of one separate trial. Each dot display shows 10 single trial responses to ten repeated odor presentations **A:** mACT response to hexanol (6ol) ten presentations of the alcohol hexanol (6ol). **B:** lACT responses to nonanal (9al). **C:** LN responses to 2-heptanone (2.7on). Grey shading represents time of odor presentation (2 s). Blue bars indicate response strength in rate [1/s].

tory interneuron responses to multiple-trial presentations of the same olfactory stimulus. All PNs responded reliably (100 %, r = 1) to multiple-trial presentations of the same odor with little difference in response strength (Fig. 2A, B). Since LNs showed a much lower response strength than the PNs, response detection (see Materials and Methods) was rather difficult. As depicted in Figure 2C, responses could be detected but exhibited different time courses leading to different response strengths across trials. Thus olfactory PNs responded reliably to multiple presentations of the same odor, whereas LNs responded with varying response strengths.
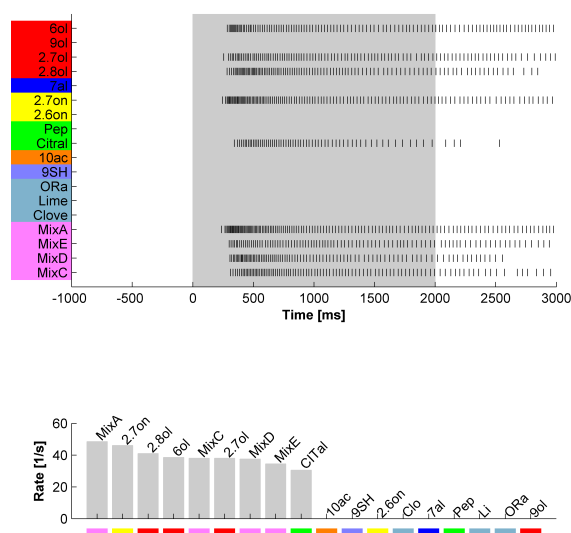
Figure II.3:
mACT odor generalization. The raster plot shows excitatory responses to 9 out of 18 odors tested and neutral responses to 9 out of 18 odors tested ($g_{ex} = 0.50$). The response strength (bottom) measured during odor stimulation (grey shading, 2 s) is rather similar for individual effective odors. Color patches represent different chemical classes of single compound odors or odor mixtures. Red = alcohol, dark blue = aldehyde, yellow = ketone, green = terpene, orange = acid, light blue = sulfur, grey-blue = complex mixtures, purple = tertiary mixtures.

Odor Generalization   We defined odor generalization as the relative number of odors that evoked either an excitatory nor an inhibitory reponse. We applied single-trial presentations of multiple single compound odors and odor mixtures and calculated the generalization index g for each olfactory interneuron (Table
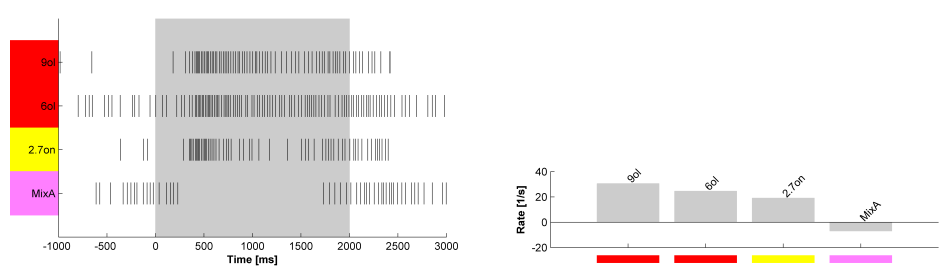
Figure II.4:
lACT odor generalization. The raster plot shows excitatory responses to 3 out of 4 odors tested and 1 inhibitory response ($g_{ex} = 0.75$, $g_{in} = 0.25$). The response strength (bottom) measured during odor stimulation (grey shading, 2 s) is similar for odors eliciting an excitatory response and lower in comparison to the spontaneous activity for the inhibitory response. Color patches see Figure 3.

Figure II.5:
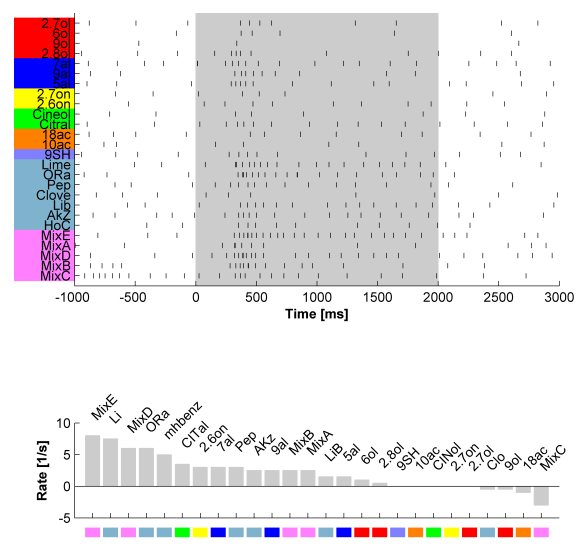LN odor generalization. The rater plot shows excitatory response to 17 out 26 odors tested and neutral responses (could not be identified as inhibitory response due to the minor difference compared to the spontaneous activity) to 9 out of 26 odors testes ($g_{ex} = 0.65$). The tuning curve (bottom) shows the response strength measured during odor stimulation (grey shading, 2 s).Color patches see Figure 3.

1, inhibition = g_{in}; excitation = g_{ex}) . Figures 3, 4 and 5 show examples of a m-, lACT and LN olfactory responses to single-trial presentations of different odors. The PNs showed odor-specific excitatory and inhibitory responses (Fig. 3A, Fig. 4A) most frequently, with a high response strength up to 60 Hz (Fig. 3B, Fig. 4B). Regarding odor identity as hydrocarbon chain length or functional group, the PNs showed the most excitatory responses to alcohols (depicted in red) independent of hydrocarbon chain length. The mACT in Figure 3 shows high response strengths to 2-octanol (2,8ol) and to hexanol (6ol). The lACT in Figure 4 shows the highest response strengths to nonanol (9ol) and hexanol (6ol). The LNs, unlike the PNs, showed in general a much lower spike rate and, in addition, a higher response strength variability across odors (Fig. 5). Responses with the highest spike rates were elicited by the tertiary mixtures (purple) and complex mixtures (grey blue). As shown in Table 1, on average mACT show a $g_{in} = 0.02$ and a $g_{ex} = 0.74$. lACT PNs show a $g_{in} = 0.14$ and a $g_{ex} = 0.54$. We did not observe clear inhibitory responses in LNs, but on average they showed a $g_{-}ex = 0.65$. Consequently our results showed that odor generalization in terms of excitatory responses is similar across olfactory interneurons but differs regarding inhibitory responses.

	neuron	No. of odors	gi$_{in}$	gi$_{ex}$	lat [ms]
mACT	T202	12	-	0.42	279
	T203	30	-	0.40	281
	T316	4	-	0.75	315
	T356	4	-	0.75	335
	T345	1	-	(1)	233
	T318	2	-	1	245
	T309	4	-	1	257
	T364	1	-	(1)	375
	T368	4	0.25	0.75	329
	T331	1	-	(1)	289
	T357	14	0.21	0.15	429
	T358	4	-	1	260
	T206	18	-	0.50	238
	mean				287 ±60
	14	5	-	1	307
	15	5	-	0.80	354
	16	2	-	0.50	444
	17	1	-	(1)	254
	18	4	-	0.75	211
	19	11	-	0.81	251
	20	3	-	1	358
	21	8	-	0.88	249
	22	11	-	1	270
	23	13	-	0.61	231
	mean		0.02	0.74	

	neuron	No. of odors	gi_{in}	gi_{ex}	lat [ms]
lACT	T139	9	-	0.22	138
	T133	12	-	1	216
	T109	4	-	0.5	134
	T122	24	0.25	0.38	262
	T142	3	-	0.67	225
	mean				195 ±57 ∓
	6	4	0.5	0.25	452
	7	4	0.25	0.75	311
	mean		0.14	0.54	
LN	1	5	-	1	262
	2	3	-	1	247
	3	26	-	0.77	280
	4	12	-	0.5	246
	5	9	-	0.89	214
	6	4	-	0.25	259
	7	15	-	0.13	184
	mean		0	0.65	241 ±32

Table II.1:

Response generalization indices (g_{in} = inhibitory responses, g_{ex} = excitatory responses) and latencies (lat, [ms]) of mACTs (N = 23), lACTs (N = 7) and LNs (N = 7). ∓ indicates significant difference between the mean latencies of identified m- and lACTs (Wilcoxon rank-sum, p < 0.01)

Response latency   To account for different temporal dynamics in odor coding of olfactory interneurons we calculated the response latency (lat) of individual neurons as the average latency to all odors eliciting an excitatory response (see Materials and Methods). Figure 6 shows the response rate estimated for m-,
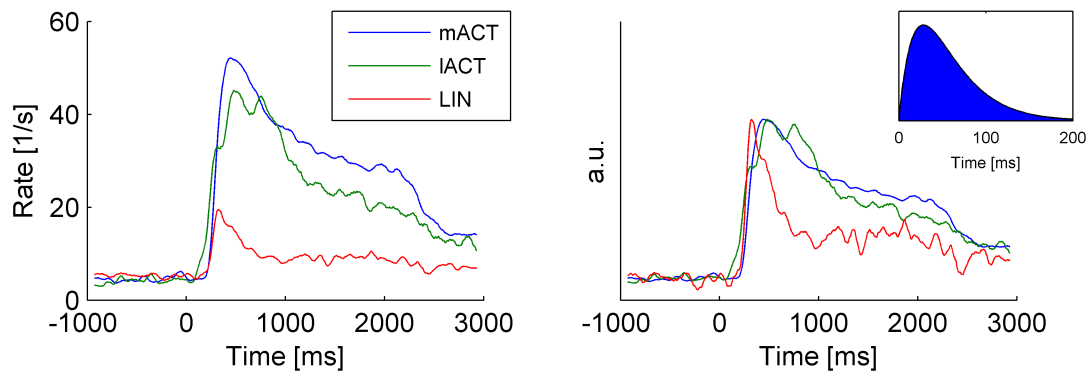
Figure II.6:
Average response profiles for identified mACTs (blue, N = 13), lACTs (green, N = 5) and LNs (red, N = 7). Inset depicts the α function used for rate estimation (see Materials and Methods). lACTs show a shorter latency in comparison to mACTs and LNs (left). Normalization to the total response strength (right) defined as the area from response onset until the end of the stimulus showed that LNs exhibit a shorter phasic component in their response in comparison to the PNs.

lACTs and LNs averaged across all neurons (see Table 1 for latencies of individual interneurons). lACTs showed a shorter response latency in comparison to mACTs and LNs (Fig. 6, left). Normalization to the total response strength defined as the area from response onset until the end of the stimulus showed that LNs exhibit different temporal dynamics in comparison to m- and lACT in terms of a much shorter phasic component (Fig. 6, right). The statistical analysis of identified PNs revealed that lACTs exhibit a significantly (Wilcoxon rank-sum, $p < 0.01$) shorter response latency (mean $\pm$ SD, 1955 $\pm$ 7 ms) than mACTs (287 $\pm$ 60 ms). The response latency of LNs was similar to the latency observed in mACTs (241 $\pm$ 32).

Hence we could show that LNs exhibit different response time courses (shorter phasic component) in comparison to PNs. Considering the response onset, our results showed that lACT have a shorter response latency than mACTs and LNs.

Spatial activity patterns within a neural olfactory space The former results showed that PNs either respond to an odor (excitation or inhibition) with little difference in response strength or that they remain silent (neutral response).
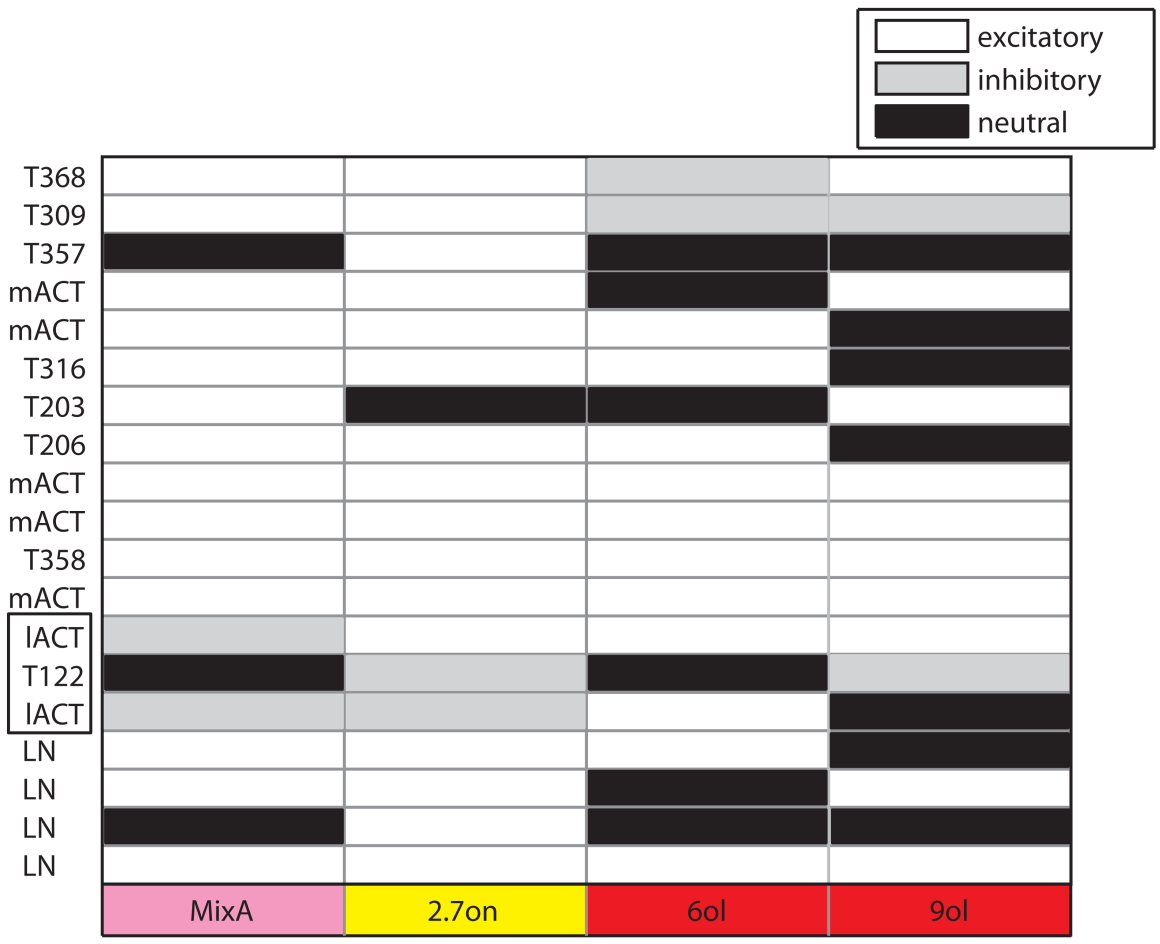
Figure II.7:
Spatial representation of olfactory interneuron responses (excitation = white and inhibiton = grey) or silence (black = neutral response). Y-axes represents the neural space (PNs either identified by their glomerulus or by recording site and spike pattern, LN identification by their morphology or spike pattern). X-axes represents the odor space: tertiary mixture (MixA) and its elemental components the ketone 2-heptanone (2.7on) and the alcohols hexanol (6ol) and nonanol (9ol). The matrix shows that a combinatorial pattern represented by responses (excitation, inhibition) or silence (neutral) is sufficient to encode odor identity. Note the most inhibitory lACT (black square) odor mixture responses.

According to the neuronal space within the AL we established a simplified model of single olfactory interneuron activity patterns. We defined a neural space of the antennal lobe represented by m-, lACTs and LNs in which the same set of odors was tested. This odor space was represented by the tertiary mixture Mix A and its elemental components 2-heptanone (2.7on), hexanol (6ol) and nonanol (9ol). Figure 7 shows a simplified matrix of olfactory activity patterns across m-, lACTs and LNs within the antennal lobe. Odor identity is represented by combinatorial activity patterns of either responses (white = excitation, grey = inhibition) or silence (black = neutral response). Focussing odor responses across the neuronal space our results showed that mACTs exhibit an odor-specific combinatorial pattern with mostly excitatory responses – in particular to the tertiary mixture Mix A and the ketone 2-heptanone (Fig. 7). Unlike the mACTs, the lACTs most frequently showed inhibitory responses, in particular to the tertiary mixture Mix A (Fig. 7, black square) which was also observed for some other mixtures tested (data not shown). The LNs stayed either silent or showed excitatory responses across all odors.

Thus we could show that mACTs code odor identity in terms of odor-specific combinatorial patterns of mostly excitatory responses, whereas lACTs showed mixture-specific inhibition.

Odor mixture encoding in olfactory interneurons Since our results showed that PN and LN olfactory activity patterns differ regarding an odor mixture and its elemental components we tested the phenomenon of mixture interactions (see Materials and Methods). We defined the most effective component of the mixture (2- heptanone, hexanol or nonanol) by the elicited response strength and compared it to the mixture response. The odor mixture response was divided into three categories: higher (synergy), equal (hypoadditivity) or lower (suppression) than the response to the most effective component (for further details see Materials and Methods). We were thus able to the issue of how the re-
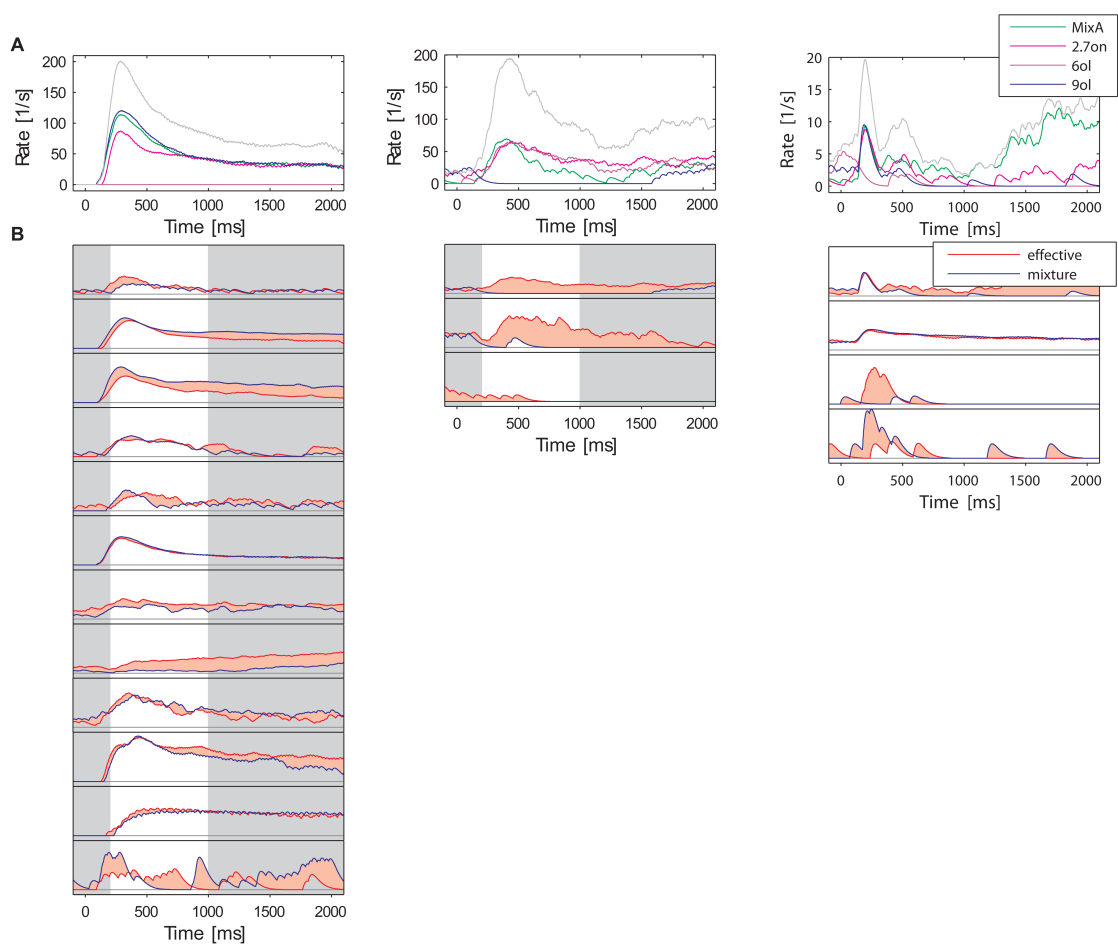
Figure II.8:
Single compound odor and odor mixture responses of mACTs (N = 12), lACTs (N = 3) and LNs (N = 4). **A** depicts average response profiles of one example. The grey line represent the linear sum of the single compound responses. Mix A = green, 2.7on = pink, 6ol = red, 9ol = blue. **B**: Each the average response profile represents one single neuron. The red line indicates the average response profile to the strongest (most effective) component. The blue line depicts the average response profile to the mixture. The red patch depicts the response difference between mixture and most effective component measured within a fix window from 200 ms to 1000 ms (white) with respect to spike counts. The mACTs (left column) show hypoadditive mixture response. The lACTs (central column) show suppressive mixture responses. The LNs (right column) show hypoadditive (first and second example), suppressive (third example) and synergistic (fourth example) mixture responses.

sponse to a mixture is related to the responses to its elemental components. Figure 8 shows the dynamic response profiles of individual olfactory interneurons elicited by the tertiary mixture Mix A (Fig. 8A, green) and its components the ketone 2-heptanone (Fig. 8A, pink), and the alcohols hexanol (Fig. 8A, dark red) and nonanol (Fig. 8A, blue). We calculated the linear sum of the single compound odor responses (Fig. 8A, grey line) and compared it to the observed response elicited by the mixture. Quantitatively, our results showed that the linear sum of single compound odor responses exceeded the measured odor mixture response for PNs and LNs respectively (Fig. 8A). Considering the three categories of odor mixture responses in comparison to the most effective odor response our results showed differences among the PNs and, in comparison, the LNs (Fig. 8B). In the majority of cases mACTs showed hypoadditivity where the response to the mixture resembled the response of the most effective component (Fig. 8A and B, left). The lACTs, in contrast to the mACTs, most frequently showed inhibitory responses to the mixture (suppression) and excitatory responses to its elemental components (Fig. 8A and B, center). We calculated κ as the relative response difference between the mixture and its most effective component (see Materials and Methods). Since we found hypoadditivity effects for mACTs the mean $\kappa = -0.103$, whereas lACTs showed a mean $\kappa = -0.913$, identifying suppressive effects. LNs showed different categories of mixture interactions. The first two examples in Figure 8B (right) show hypoadditivity, since the odor mixture and most effective component responses are similar. The third example shows a lower mixture response in comparison to the most effective component response; the last example shows synergy in terms of a higher odor mixture response than the most effective component response.

In general our results revealed that odor mixture responses cannot be predicted from the knowledge about their elemental component responses. Considering m-, lACTs and LNs we could show that mACT odor mixture responses

can be predicted from the most effective odor response, whereas lACT odor mixture responses cannot. LNs showed different categories of mixture interaction, indicating more complex mixture encoding mechanisms.

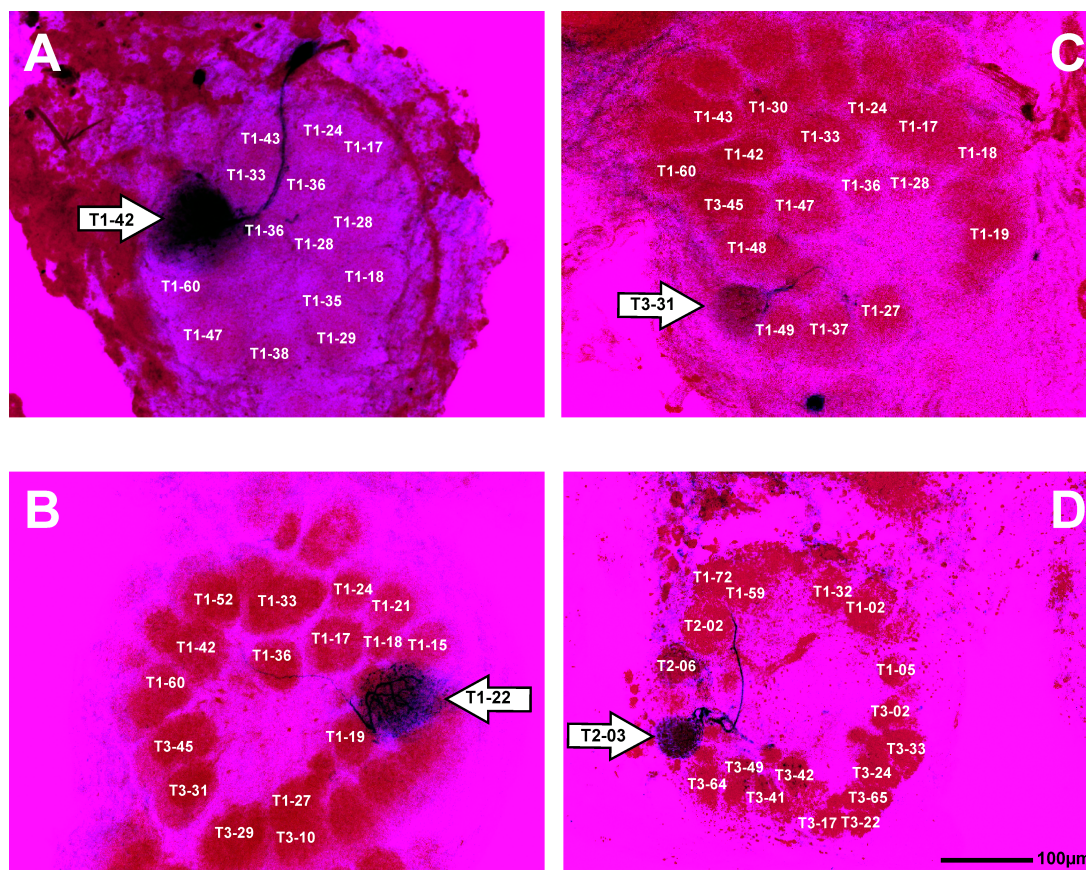## Spatial representation of projection neuron in- and output

Figure II.9:
Identification of l- and mACTs by their uniglomerular projections within the antennal lobe. Inverse shadow projection of single marked projection neurons (blue) and the neuropil counterstaining (red). Landmark glomeruli are depicted by their identification according to the honeybee antennal lobe atlas (white text). PN input (uniglomerular arborization) is indicated by a white arrow. **A:**lACT with uniglomerular projections within the T1-42 glomerulus. **B:**lACT with uniglomerular projections within the T1-22 glomerulus. **C:**mACT with dense arborization within the T3-31 glomerulus. **D:**mACT with dense aborization within the T2-03 glomerulus.

Based on our findings, mACTs and lACTs differ regarding their odor-identity and odor mixture encoding mechanisms. Besides their odor-encoding strategies we visualized their anatomical features by applying intracellular staining,

3-D reconstruction and mapping techniques (see Materials and Methods). This allowed us to relate l- and mACT input and output sites to their functional properties and to visualize multiple PNs in one reference system, the Atlas of the Honeybee Brain. PNs were identified according to their uniglomerular arborizations within the antennal lobe representing their input site. Figure 9 A - D shows four examples of uniglomerular PNs identified as either m- or lACTs according to the honeybee antennal lobe atlas (Galizia et al., 1999). This atlas represents each glomerulus identified by the OSN tract which innervates it (T1 - T4) and each PN was numbered and assigned to its glomerular input (T1 for lACTs and T2 - T4 for mACTs).
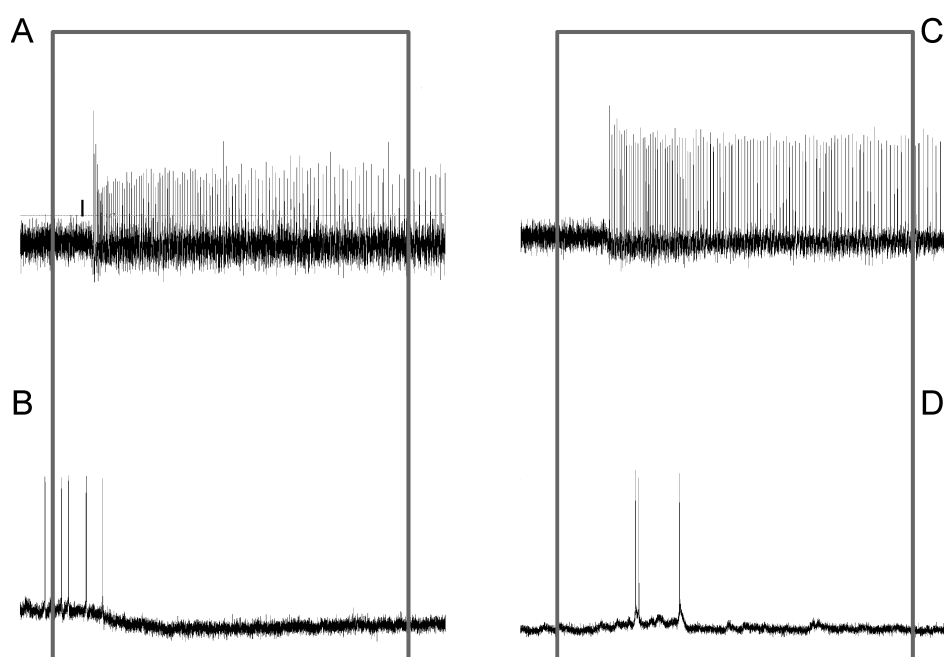
Figure II.10:
Odor responses of l- and mACT PNs to the odor 2-heptanone (grey square, stimulus duration 2 s). **A:**Excitatory response to 2.7on, T1-42 lACT. **B:**Inhibitory response to 2.7on, T1-22 lACT. **C:**Excitatory response to 2.7on, T3-31 mACT. **D:**Neutral response (spike represent spontaneous activity) to 2.7on, T2-03 mACT PN.

Figure 10 A - D shows the olfactory responses of the identified m- and lACTs to the ketone 2-heptanone. The lACT with uniglomerular arborizations within the T1-42 glomerulus (Fig. 9A) showed an excitatory response to 2-heptanone (Fig. 10A), whereas the T1-22 (Fig. 9B) lACT was inhibited by 2-heptanone

(Fig. 10B). The T3-31 (Fig. 9C) mACT showed an excitatory response to 2-heptanone (Fig. 10C), whereas the T2-03 (Fig. 9D) did not respond to the odor (Fig. 10D, the spikes depicted represent spontaneous activity). Thus m- and lACT PNs get distinct olfactory input accordant to their uniglomerular arborizations, leading to a glomerulus-specific AL output.

Both types of PNs convey olfactory information to the higher-order brain centers, the MBs. The MB calyces receive the olfactory information by PN axon terminals projecting onto the lip region. Since single m- and lACTs showed glomerulus-specific olfactory response profiles, we visualized their output sites within the MB lips represented by their axon terminals (boutons). Application of sophisticated reconstructions of single PNs and their composition within the Atlas of the Honeybee Brain allowed us to visualize a subset of PNs within a spatial reference system.

Figure 11 A and B show the calycal aborizations of projection neurons identified by their input site (Fig. 9A-D) and characterized by their olfactory response profiles (Fig. 10A-D). To relate PN in- and output we performed 3-D reconstructions of the T1-22 lACT (Fig. 11, depicted in green) as well as of the T3-31 mACT (Fig. 11, depicted in orange) and the T2-03 mACT (Fig. 11, depicted in magenta) on the contralateral site. The top view in Figure 11B shows the PN output sites within the MB lips as well as in the lateral horn. We focussed on the output sites within the mushroom body lips (Fig. 11B). The spatial assignment of single PN boutons was achieved by mapping the calycal lip neuropil of the honeybee Atlas onto the reconstructed skeleton trees of single PNs. This allowed us to visualize single PN boutons according to their spatial distribution in conjunction with their uniglomerular input. Figure 12 shows clear differences in the terminal arborization patterns of both ACTs.

The T1-22 lACT (Fig. 12, depicted in green) innervates the central core of the lip (Fig. 12, higher magnification outlines blue shows noninnervated cortical layer) whereas the T3-31 mACT (Fig. 12, depicted in orange) and the T2-03
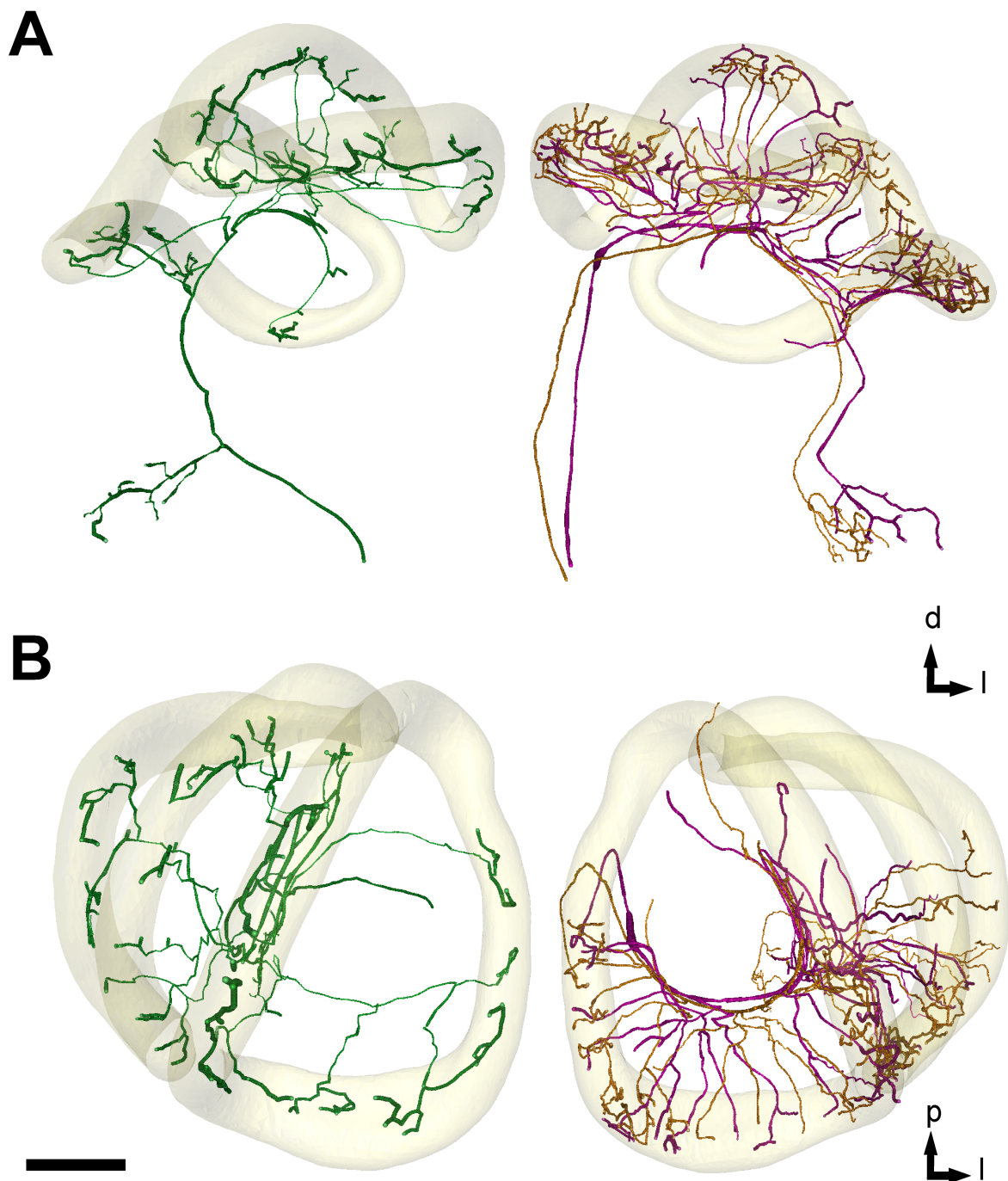
A: frontal view.

d
↑
→ l

B: top view.

p
↑
→ l

Figure II.11:
Projection neurons fitted into the Atlas of the Honeybee Brain). **A:** frontal view. **B:** top view. Green = T1-22 lACT, orange = T3-31 mACT, magenta = T2-03 mACT. Scale bar = 100 μm

mACT (Fig 12, depicted in magenta) PN innervate the whole lip region, but with different densities (Fig. 12A, higher magnification outlines black).

Thus our anatomical results revealed that l- and mACTs possess segregated aborization patterns within the MB lips and that the mACTs themselves exhibit glomerulus-specific spatial distributions of their axon terminals.
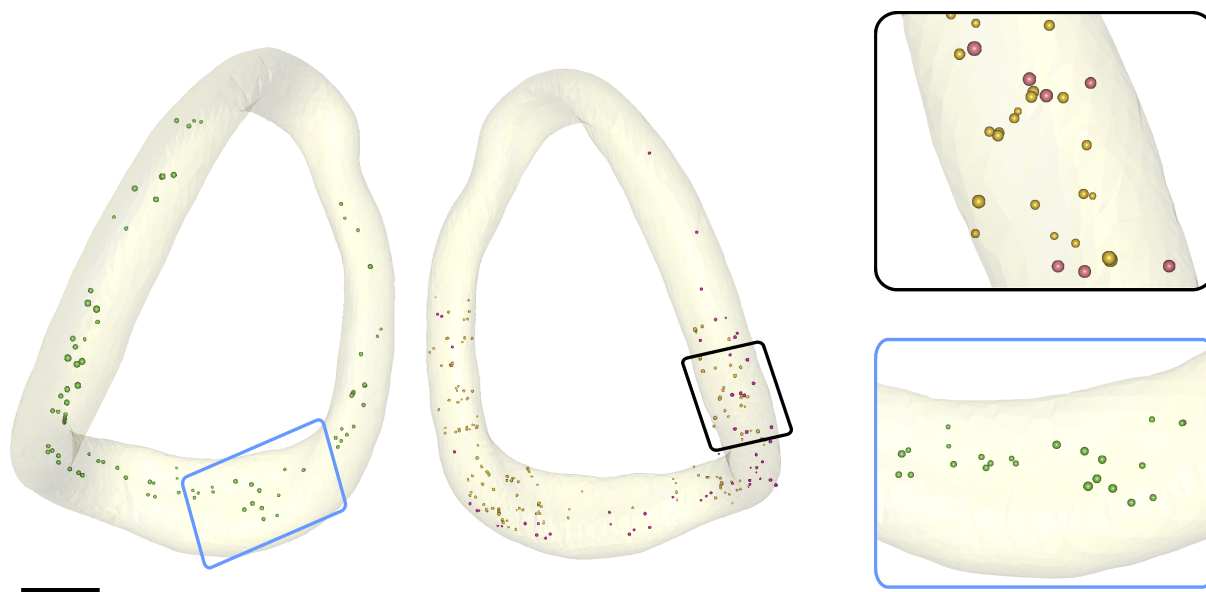
Figure II.12:
Spatial distribution of PN terminal arborization patterns within the MB lips. To visualize their patterns with higher magnification accounting for the lACT and the mACTs respectively the figure depicts solely the median lips of the MB calyces. The left panel shows the honeybee's right median lip with lACT PN boutons and left median lip with mACT PN boutons. Higher magnification outlined in blue shows lACT arborization patterns within the central core of the lip leaving the cortical layer noninnervated. Higher magnification outlined in black shows the T3-31 PN boutons (orange) and the T2-03 PN boutons (magenta) innervating the entire lip but with different densities. Scale bar = 20 µm

Discussion

By applying single-cell electrophysiological recordings, olfactory stimulations with a large and diverse set of single compound odors as well as odor mixtures (Fig. 1), and 3-D reconstructions we addressed the issue of how olfactory interneurons encode odors and whether it is related to their morphology. We provide the first analysis of functional principles in olfactory coding in relation

to anatomical features composed within a common framework, the Atlas of the Honeybee Brain.

Our results showed that PNs and LNs differ regarding their olfactory response profiles (see Table 1). PNs, in contrast to the LNs, respond more reliably to multiple-trial presentations of the same odor (Fig. 2A - C) and encode odor identity and odor mixtures in terms of spatial activity patterns represented by inhibitory and excitatory responses (Fig. 3, 4, 5 and 7). In general, PNs respond to odors with a much higher response strength and a longer phasic component than the LNs (Fig. 6). Considering the temporal dynamics of PN and LN olfactory responses we were able to show that lACTs respond to odors with a shorter latency in comparison to mACTs and LNs (Fig. 6).

Stimulations with multicompound odor mixtures revealed different odor mixture encoding strategies for mACTs, lACTs and LNs, respectively. Our results showed that odor mixture responses of mACTs and lACTs can be divided into two categories: mACTs show hypoadditive mixture encoding, whereas lACTs evince suppressive odor mixture encoding. For the LNs, unlike the PNs, our results revealed three categories of mixture interactions: hypoadditive, suppressive, and synergistic odor mixture responses (Fig 8). Thus our results led to the assumption that mACT odor mixture responses can be predicted with respect to the more effective component model (MEC) (Daniel et al., 1996), whereas lACT odor mixture responses cannot.

Mueller et al. (2002) proposed dual coding of the same odor stimulus by two different neuronal strategies represented by the m- and lACTs. Since our results showed hypoadditive odor mixture responses in mACTs and suppressive odor mixture responses in lACTs we assume that mACTs extract odor identity whereas lACTs transfer odor mixture information. Thus considering PN responses to the multicompound odor Mix A, lACTs identify the odor as a mixture, whereas mACTs extract the most effective component of the mixture, leading to the dual encoding of the same olfactory stimulus.

Recent studies on the lateral and medial olfactory tract in fish suggested that the medial tract processes pheromonal information and mediates reproductive behavior, while the lateral tract conveys information about food (Satou et al., 1983; Stacey and Kyle, 1983; Demski and Dulka, 1984; Sorensen et al., 1991; Hamdani et al., 2001; Weltzien et al., 2003). Since we tested a large and diverse set including pheromonal components as well as natural floral blends (data not shown) this consideration will be tested on the lACTs and mACTs of the honeybee. On the basis of the suppressive odor mixture response in lACTs we would hypothesize that they play a dominant role in food information processing, since bees forage on flowers associated with the perception of complex olfactory stimuli.

Considering the LNs, our results revealed hypoadditive, suppressive as well as synergistic odor mixture responses (Fig 8, right panel) which might be explained by their physiological as well as anatomical functions within the AL network. The honeybee AL exhibits two morphological types of LNs; 87 % are homogeneous, whereas 13 % are heterogeneous (Flanagan and Mercer, 1989; Fonta et al., 1993). Homogeneous LNs show arborizations within multiple glomeruli, whereas heterogeneous LNs strongly innervate a single glomerulus, and diffusely branch into several other glomeruli (Flanagan and Mercer, 1989). Corroborating our results, earlier studies showed that both LN types differentially respond to different odors (Sun et al., 1993). It has been shown that the heterogeneous LNs get their olfactory input from the glomerulus into which they branch more strongly (Galizia and Kimmerle, 2004). Hence the three categories of LN odor mixture responses observed in this study might be explained by their glomerular arborization patterns. Since PNs have distinct uniglomerular projections hypoadditive LN odor mixture responses could represent heterogeneous strong branching within a mACT input glomerulus, whereas suppressive LN odor mixture responses could be due to heterogeneous strong branching within a lACT input glomerulus. Synergistic LN odor mixture re-

sponses might represent homogeneous LNs diffusely branching within multiple glomeruli or result from LN interglomerular connections.

Our results revealed two processing channels (m- and lACT) for the encoding of odor mixtures which might be related to their elaborate anatomical features. Since m- and lACTs receive input from two clearly-defined sets of glomeruli clustered in two AL hemispheres and their projections remain largely segregated within the MB lip (Suzuki, 1975; Gronenberg, 2001; Abel et al., 2001; Mueller et al., 2002; Kirschner et al., 2006) our study was designed to relate functional m- and lACT input to their output sites within the MB lips. We identified single PN functional properties, performed 3-D reconstructions and composed them within a spatial reference map, the Atlas of the Honeybee Brain (Brandt et al., 2005). Our results showed that single m- and lACTs exhibit glomerulus-specific (Fig. 9) functional properties (Fig. 10) represented by their spatial arborization patterns within the MB lips (Fig. 11 and 12). We focused on these patterns and showed that lACTs innervate the central core of the MB lips (Fig. 12), whereas the mACTs show terminal arborization patterns throughout the entire lip but with different densities (Fig. 12). These results corroborate earlier results (Gronenberg, 2001; Kirschner et al., 2006) indicating a glomerulus-specific segregation of PN output. Thus this result indicates that olfactory information is processed from m- and lACT presynaptic terminals (boutons) onto different subsets of postsynaptic Kenyon cells (KC).

It is known that KC dendritic trees occupy domains within the MB lips (Strausfeld, 2002) that appear to reflect the organization of axon collateral endings from different classes of PNs. Certain spiny class I KC extend across the whole of the lips, whereas others are constrained to a part of the lip, lining its outer half or its outer and lower edges (Strausfeld, 2002). Clawed class II KC extend through the lip zones, each having a narrow columnar dendritic domain (Rybak and Menzel, 1993; Strausfeld, 2002; Farris et al., 2004). lACTs exhibited shorter response latencies (Fig. 6, Mueller et al., 2002) and since it is known that clawed

KCs exhibit stable and immediate responses, it is assumed that clawed KCs are exclusively driven by l-ACTs (Szyszka et al., 2005). Thus we hypothesize that the observed sparsening of the combinatorial pattern observed in clawed KC (Szyszka et al., 2005) is related to lACT odor mixture encoding strategies. Optical imaging studies revealed that odors are represented as overlapping lACT glomerular activity patterns, whereas their boutons within the MB lips show fewer overlapping responses. According to our data we suggest that lACTs encode odor mixtures which might represent a less complex unit of information which is conveyed onto the KC. Therefore PN output activity patterns appear sparse.

Since the mACTs encode odor identity we would assume that they extract more information about elemental components which refer to a more complex read-out by the KCs. Since our anatomical data showed that mACT boutons are distributed throughout the entire lip (Fig. 12) a pattern which resembles the anatomical features of class I KCs (Strausfeld, 2002), we hypothesize that different types of class I KCs might be driven by the mACTs.

Encoding single compound odors and odor mixtures on the MB lip level might additionally be regulated by reciprocal and feed-forward microcircuits between GABAergic neurons and PNs (Ganeshina and Menzel, 2001). These circuits indicate that the information flow from PNs onto KCs may not only be shaped by feed-forward processes, but may include interactions between PNs and GABAergic neurons within the MB microcircuits.

However our results revealed m-, lACT and LN odor identity and odor mixture encoding strategies on the level of the first-order relay station, the AL. The issue of how the olfactory code is computed on the level of the second-order relay station, the MB, must still be addressed, but our study suggests that m, and lACTs convey olfactory information onto different subsets of KC, presumably influencing olfactory coding.

The elucidation of olfactory computation within different processing levels

of the olfactory pathway the AL and the MB in relation to the morphology of neurons within the accordant networks still remains a sophisticated task. Opto-physiological and electron microscopical studies will be necessary to determine synaptic transmission between presynaptic m- and lACT boutons and their accordant postsynaptic elements, the KC spines. Anatomical features have to be determined in a more elaborate way by combining single-cell markings with electronmicroscopy (Ganeshina and Menzel, unpublished) and two-photon microscopy (Wachowiak et al., 2004, Franke and Menzel, personal communications). The Standard Atlas of the Honeybee Brain will facilitate the understanding of olfactory encoding and enrich our understanding of individual neurons forming a complex network.